

Chemisorption and Physisorption of Water Vapors on the Surface of Lithium-Substituted Cobalt Ferrite Nanoparticles

Pradeep Chavan*



Cite This: *ACS Omega* 2021, 6, 1953–1959



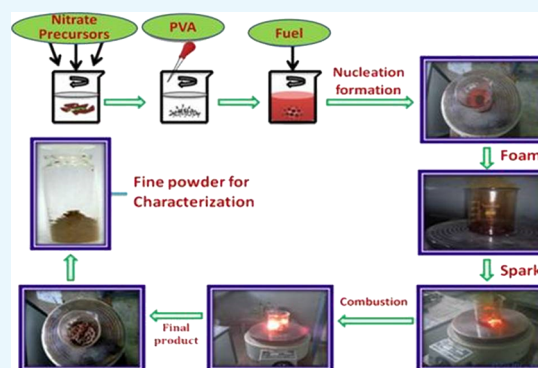
Read Online

ACCESS |

Metrics & More

Article Recommendations

ABSTRACT: Ferrimagnetic materials have the assembly of n-type porous semiconductors that shows the evidence of several physical properties used in electronic devices and technology. If the water vapors are brought closer to the surface of n-type semiconductors, then the electrons near the surface of materials are transferred from the conduction band to the electron-accepting level of the water molecule that provides chemisorbed layer of OH^- ions. The conduction of electrons takes place only when H_3O^+ releases one proton to the nearest water molecule that accepts electrons while releasing another proton and so on. This mechanism is known as the Grotthuss chain reaction; it is the essential conduction mechanism of water and surface layers of water on the humidity-sensitive semiconducting materials. In this article, the humidity-sensing properties of Li-substituted cobalt ferrite nanoparticles prepared by the solution combustion method are reported. The result of the data suggested that the substitution of Li ions improved the formation of smaller grains of cobalt ferrite, which results in a rise within the surface area and improved the humidity sensitivity of ferrite nanoparticles.



INTRODUCTION

The improvement of scientific applications of n-type semiconducting materials in modern technology is significant to assemble extremely sensitive, steady, and cheaper humidity-sensitive devices to manage the humidity level for processing tremendously sophisticated electrical circuits in electronics engineering.¹ The growing demand of programmed devices needs smart humidity-sensitive devices to regulate the livelihood environment circumstances; the humidity sensitivity can influence our normal life in numerous customs like human comforts, preserving and processing food, physical and chemical processes in pharmaceuticals, plantation conditions, weather prediction, and so on.^{2–5} To watch and control the humidity level are of consequence from the previous couple of decades, the consideration of the event of extremely humidity-sensitive semiconducting materials that have huge technological applications.⁶

Numerous outstanding chemical and physical phenomena that happened on the surface of ceramic materials rely on the surface of conduction of electrons and porous structure.⁷ In view of that fact, the adsorption of water vapors can take place on the surface of ceramic materials because of the chemical reactivity of porous materials; consequently, the electrical conductivity increases. Accordingly, the rise of electrical conductivity of porous materials with reference to humidity sensitivity was due to the chemisorption and physisorption of the water vapors on the surface of porous semiconducting materials.⁸ If water vapors

are brought closer to the surface of n-type semiconducting materials, then the electrons on the brink of the material surface are transferred from the conduction band to the electron-accepting level of the water molecule that provides chemisorbed layers of OH^- ions.⁹ Thus, the conduction mechanism of electrons takes place only when H_3O^+ releases one proton to the adjacent water molecule that accepts the electrons while releasing another proton, and so on. Such mechanism is called as the Grotthuss chain reaction mechanism¹⁰; Grotthuss chain reaction is the fundamental conduction mechanism of water and water surface layers on humidity-sensitive materials.

The ferrite nanoparticles synthesized with the help of a solution combustion method that helps in getting controlled smaller crystallite sizes and enhancing the properties of nanoparticles. Also in this method, it easily controlled the grain growth, grain size, and sintering temperature for particular applications. In this article, the humidity-sensing mechanism of Li-substituted cobalt ferrite nanoparticles synthesized by using solution combustion method of inorganic reagents of metal

Received: September 29, 2020

Accepted: January 4, 2021

Published: January 13, 2021



nitrates is reported. The foremost important motivation for substituting Li ions was to get supplementary defects and porosity into the structure of ferrites. The results recommended that the substitution of Li ions enhanced the configuration of smaller grains of cobalt ferrite, which results in a rise within the surface area and enhanced the humidity sensitivity of ferrite nanoparticles.

CHARACTERIZATION DETAILS

XRD measurement was carried out by using an X-ray diffractometer with Cu $K\alpha$ radiation having a wavelength of 1.5406 Å. AFM characteristics have been carried out by using the Nanosurf Easyscan2 at USIC, KUD. DC resistivity with respect to relative humidity response was measured by using the two-probe method within the range from 10 to 90% RH at room temperature. Therefore, porosity of the ferrite nanoparticles was projected by using Hendricks and Adam's method¹² from the following equation:

$$\% \text{porosity} = \frac{(d_x - d_a)}{d_x} \times 100 \quad (1)$$

where d_x = X-ray density and d_a = actual density.

The actual density of the samples was determined with the help of the radius, thickness, and mass of the pellet, i.e., d_a = mass/volume. X-ray density was calculated from the values of the lattice parameter using the formula $d_x = \frac{8M}{Na^3}$, where 8 represents the number of molecules in a unit cell of spinel lattice, M is the molecular weight of the ferrite sample, N is Avogadro's number, and a is the lattice constant. The relative humidity is generated by using the two-pressure technique in the relative humidity generator on the idea of the subsequent equation¹⁰

$$\% \text{RH} = \frac{P_a}{P_s} \times 100 \quad (2)$$

where P_a = actual pressure of water vapor at room temperature and P_s = saturation pressure of water vapor. The humidity sensitivity factor was estimated by using the following equation:

$$S_f = \frac{R_{90\%}}{R_{10\%}} \quad (3)$$

RESULTS AND DISCUSSION

The development of the spinel segment of $\text{Li}_x\text{Co}_{1-x}\text{Fe}_2\text{O}_4$ nanoparticles for various concentrations of Li was confirmed by XRD measurement shown in Figure 1; the whole recorded spectra were analogous to the cubic spinel structure of Li-substituted cobalt ferrites and indexed with the assistance of "American Society for Testing and Materials" (ASTM) data, which confirmed the formation of single-phase cubic spinel structure without any impurities in all the samples. The average crystallite size was estimated by using Scherer formula¹¹: $D = \frac{0.89\lambda}{\beta \cos\theta}$; the calculated average crystallite sizes are listed in Table 1. It is observed that the crystallite size increases with increasing Li concentration in cobalt ferrites; it is because of the chemical composition, grain growth, ionic radius, porosity, and impurities. The crystallite size increases within the range from 26.32 to 48.59 nm.

The AFM micrographs exhibited some dissolved ferrite nanoparticles that precipitated during the cooling process to form hardly resolvable particles, which had lacking time to

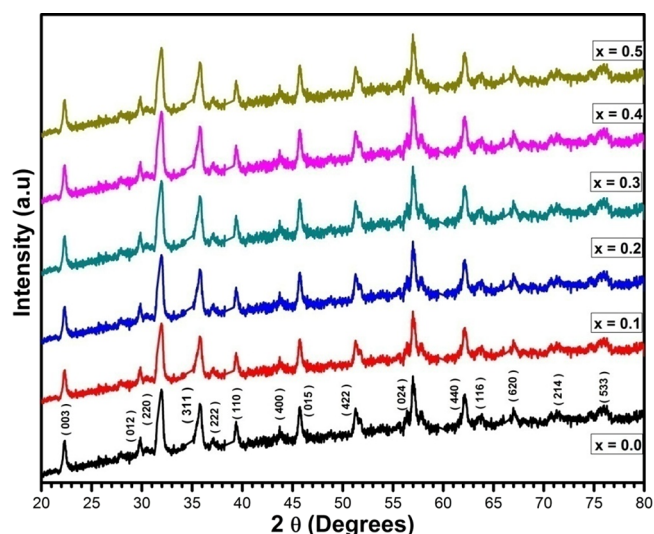


Figure 1. XRD characteristics of Li-substituted cobalt ferrite nanoparticles calcined at 800 °C (x represents the Li concentration).

Table 1. Structural Characteristics, Electrical Resistance, and Sensitivity Factor of Li-Substituted Cobalt Ferrite Nanoparticles (x Represents the Li Concentration)

x content	average crystallite size (nm)	grain size (nm)	lattice constant (nm)	% porosity	log R (Ω)	sensitivity factor
0.0	26.32	38.26	0.72	30.26	7.373	605.21
0.1	30.15	46.69	0.79	26.62	7.06	652.15
0.2	35.26	52.95	0.82	23.62	6.99	965.95
0.3	39.65	59.56	0.84	19.26	7.15	1055.15
0.4	43.95	64.02	0.86	17.02	7.51	1165.65
0.5	48.59	69.85	0.89	15.65	7.26	1275.64

migrate the grain boundaries. The substitution of Li^+ ions reveals the distribution of grain size from 26.32 to 48.59 nm. Hence, it exhibits the dissolution of Li^+ ions in the cubic spinel lattice that facilitate a quicker nucleation process, leading to the distribution of smaller grain size. Therefore, the pore size distribution was smaller than the pure ferrite sample. Surface morphology showed that the grains were well connected through grain necks. This is because of the Li^+ ion concentration beyond its solubility limit in the cubic spinel lattice and formed copper ferrite.

However, the authentication of phase development of the ferrite nanoparticles by XRD measurement rests on the precise measurement of the lattice constant. The lattice constants of the ferrite nanoparticles are computed by using the " d " value and respective (hkl) parameters. From Table 1, it is observed that the lattice constant estimated from the synthesized ferrite nanoparticles is found to be 0.72 nm and gradually increases by increasing Li concentration in cobalt ferrites. The increasing trend within the lattice constant value was observed due to the slighter Li^+ ions (0.74 Å) that agglomerated with Fe^{3+} ions (0.645 Å) and Co^{2+} ions (0.65 Å).¹⁰

Thus, porosity is the inherent segment in semiconducting materials synthesized by the technique of calcination and powder processing. The high rate of calcination with small crystallite size reduces the porosity substantially. From Table 1, it is observed that the porosity decreases with an increasing Li concentration in cobalt ferrites; it is because of the grain growth, chemical composition, and ionic radius of the elements present in the ferrite system. The highest porosity (30.26%) was

observed for CoFe_2O_4 , afterward the porosity decreases continuously with increasing Li concentration. With the addition of Li ions, intergranular porosity decreases and grain size distribution changes. Therefore, the small pores are interconnected with large pores through grain necks. Therefore, a high porosity and large surface area are advantageous for improved humidity sensitivity properties of the ferrites.

Figure 2 shows the AFM micrographs of the synthesized Li-substituted cobalt ferrites measured by using non-contact mode

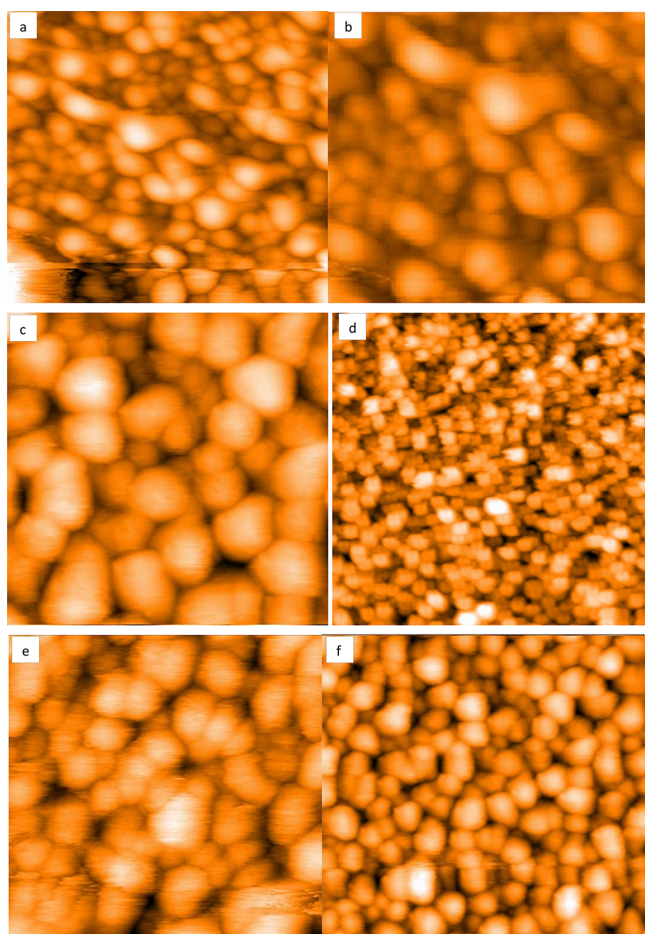


Figure 2. AFM micrographs of the synthesized Li-substituted cobalt ferrite nanoparticles ($x = 0.0, 0.1, 0.2, 0.3, 0.4,$ and 0.5 represent the Li concentration).

(dynamic mode). Micrographs reveal that the synthesized samples have a spherical shape with an average grain size that increases with increasing Li concentration. The average grain sizes of ferrite nanoparticles completely depend upon the chemical composition, the preparation condition, sintering temperature, secondary phases, and agglomeration behavior of the grains. From Figure 2, the estimated average grain sizes of the ferrite samples are listed in Table 1; the largest grain size of about 69.85 nm was achieved for $\text{Li}_{0.5}\text{Co}_{0.5}\text{Fe}_2\text{O}_4$ ferrite nanoparticles. The increasing trend of the average grain size was observed due to the agglomeration of Li^+ ions with Co^{2+} ions and Fe^{3+} ions and therefore, the expansion of the spinel lattice reaches its maximum at the composition of $x = 0.5$. Therefore, the grain sizes of the synthesized ferrite nanoparticles estimated from the AFM technique are in good agreement with the grain sizes determined from XRD using Scherer formula.

From Figure 3, the variation of DC resistivity with respect to temperature of Li-substituted cobalt ferrite nanoparticles is

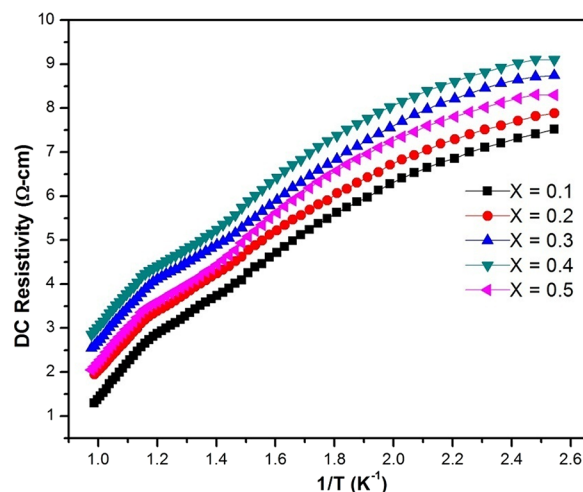


Figure 3. Variation of DC resistivity with the temperature of Li-substituted cobalt ferrite nanoparticles (x represents the Li concentration).

shown. It is observed that DC resistivity decreases with increasing temperature reveals the semiconducting behavior of ferrite nanoparticles; it is also due to the rise in drift mobility of electrical charge carriers and mostly depends on density, porosity, grain size, chemical composition, and so on.¹⁰ The decreasing trend of DC resistivity with increasing temperature was due to the hopping of conduction of electrons from Fe^{2+} to Fe^{3+} ions.

On the other hand, the conduction mechanism of the electrons was explained on the bases of the Verwey and de Boer mechanism¹² that involve the exchange of electrons between the ions of comparable elements present in more than one valence state and indiscriminately dispersed in more than the corresponding crystallographic lattice sites. Consequently, the exchange of electrons between $\text{Fe}^{2+} \leftrightarrow \text{Fe}^{3+} + e^-$ is the n-type charge carrier, and therefore, the exchange of holes between $\text{Co}^{3+} \leftrightarrow \text{Co}^{2+} + e^-$ is liable for p-type charge carriers. As a result, the decrease in DC resistivity with increasing temperature was due to the changes in cation distribution and difference in ionic size of the cations present in the ferrite system.¹⁰

The humidity-sensing characteristics of ferrite nanoparticles calcined at the temperature 800 °C with %RH dependence of the dielectric constant of ferrite nanoparticles at different Li concentrations measured at 1 kHz are shown in Figure 4. It is observed from Figure 4 that the dielectric constant increases with increasing %RH, but the dielectric constant increases with an increasing Li concentration in cobalt ferrite nanoparticles.¹³ For that reason, Li ion substitution is accomplished the development of humidity sensitivity property of cobalt ferrite nanoparticles. The dielectric constants observed at 90% RH are 6.32 ($x = 0.0$), 6.53 ($x = 0.1$), 6.65 ($x = 0.2$), 6.71 ($x = 0.3$), 6.78 ($x = 0.4$), and 6.90 ($x = 0.5$) for all the concentrations of Li ions in cobalt ferrites. Hence, it reveals that as the Li ion concentration increased, the humidity sensitivity of the ferrite nanoparticles also increased.¹⁴

Figure 5 shows the percentage of relative humidity (%RH)-dependent dielectric constant of Li-substituted cobalt ferrite nanoparticles measured at different frequencies like 20 Hz, 1 kHz, 10 kHz, and 1 MHz, and 10 MHz. From the plot, it is

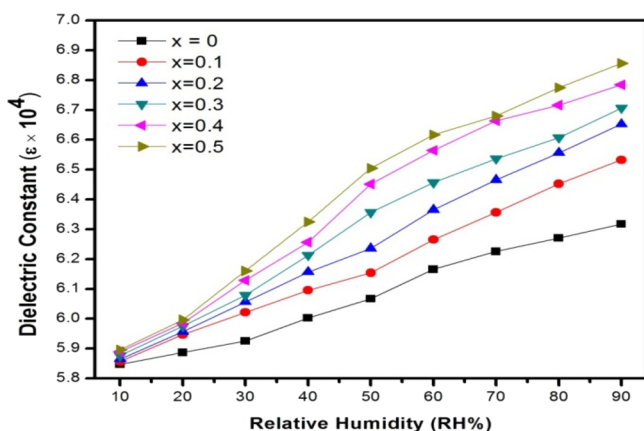


Figure 4. Humidity-sensing characteristic of ferrite nanoparticles calcined at 800 °C: %RH dependence of dielectric constants of ferrite nanoparticles measured at 1 kHz (x represents the Li concentration).

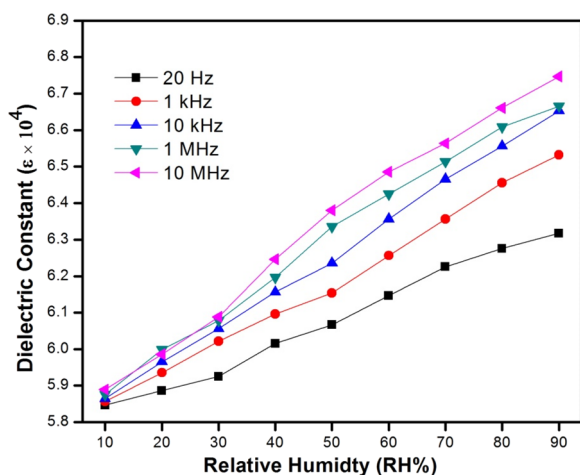


Figure 5. Humidity-sensing characteristic of pure cobalt ferrite nanoparticles ($x = 0.0$) calcined at 800 °C: %RH dependence of dielectric constants at 20 Hz, 1 kHz, 10 kHz, 1 MHz, and 10 MHz.

observed that the dielectric constant increases with increasing % RH for all the ferrite samples; it reveals that the humidity sensitivity of the ferrite nanoparticles is low at low %RH and then increases rapidly at high %RH.¹⁵ Furthermore, the humidity sensitivity increases with increasing frequency. As a result, the entire changes in the dielectric constant are found to be increased for various frequencies like 20 Hz, 1 kHz, 10 kHz, 1 MHz, and 10 MHz respectively. The behavior of response and recovery time of a pure cobalt ferrite sample is significant for the performance of humidity sensitivity measurement. Accordingly, the adsorption process is a condensation phenomenon, and the desorption process is an evaporation phenomenon of the vapors of water molecules. The adsorption and desorption process of the relative humidity hysteresis curve of pure cobalt ferrite nanoparticles is shown in Figure 6. For the measurement of the relative humidity hysteresis curve at room temperature, the humidity sensitivity was assorted within the steps of 10% RH (10–90% RH) by taking 10 min of time in each step and 5 min of time was permitted to urge the steady reading of the sample resistance, respectively. This procedure was followed together for up and down cycles of a standard relative humidity generator at room temperature. A similar procedure was followed for adsorption and desorption of water vapors.

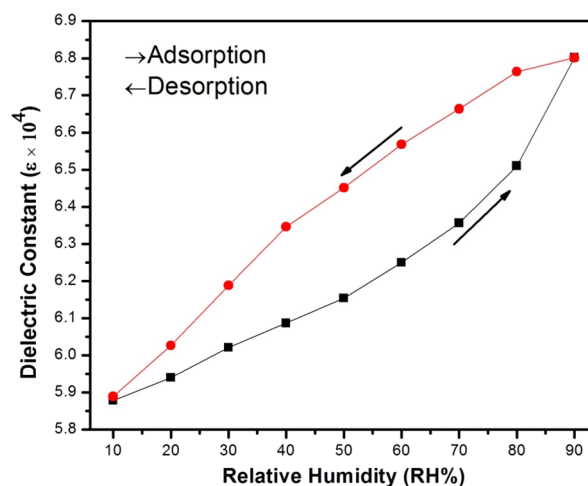


Figure 6. Humidity-sensing characteristic of pure cobalt ferrite nanoparticles calcined at 800 °C: humidity hysteresis measured at the frequency 1 kHz.

Figure 6 shows the response time curves of adsorption/desorption of pure cobalt ferrite.¹⁶ Therefore, the sum of time mandatory to succeed in a 90% rate of total change in relative humidity is the response time in case of adsorption process or recovery time in case of desorption process.¹⁷ The graph plotted for response and recovery time of pure cobalt ferrite nanoparticles calcined at 800 °C and measured at the frequency of 1 kHz is shown in Figure 6. It is observed that the pellet samples of pure cobalt ferrite nanoparticles reveals faintly large hysteresis behavior. The hysteresis error of the ferrite samples was calculated from the subsequent equation (eq 4):

$$\gamma_H = \pm \frac{1}{2} \left(\frac{\Delta H_{\max}}{F_{FS}} \right) \quad (4)$$

where ΔH_{\max} = output of maximum difference in forward and backward operation and F_{FS} = full scale output.

The highest definite quantity or saturated value of humidity hysteresis error (γ_H) of pure cobalt ferrite nanoparticles calcined at 800 °C is for 90% of relative humidity. The calcined temperature can manipulate the response properties of the ferrite nanoparticles. Therefore, the dielectric constant of pure cobalt ferrite nanoparticles at 90% relative humidity is greater than those at 10% relative humidity, respectively; the utmost dielectric constant 6.8 was observed at a 1 kHz frequency.¹⁷ The response time of the dielectric constant with respect to %RH of pure cobalt ferrite nanoparticles calcined at temperature 800 °C measured in original and after storage in regular atmosphere for about 1 year is shown in Figure 7. It is observed that there exists a small dissimilarity in the dielectric constant even later than an extended period of time; it reveals that the properties of cobalt ferrite nanoparticles are very safe over a long period of time.¹⁷ As a result, the water molecules at room temperature are physically adsorbed and also can be desorbed by passing the dry air in a reverse process. Consequently, the performance of sluggish response time and recovery time of cobalt ferrite nanoparticles was due to the slight surface-to-volume ratio of the pellets.^{16,18} Therefore, this phenomenon has an influence on the hysteresis of humidity-sensitive devices. Supplementary efforts need to be done to enhance the response and recovery time characteristics of the cobalt ferrite nanoparticles.

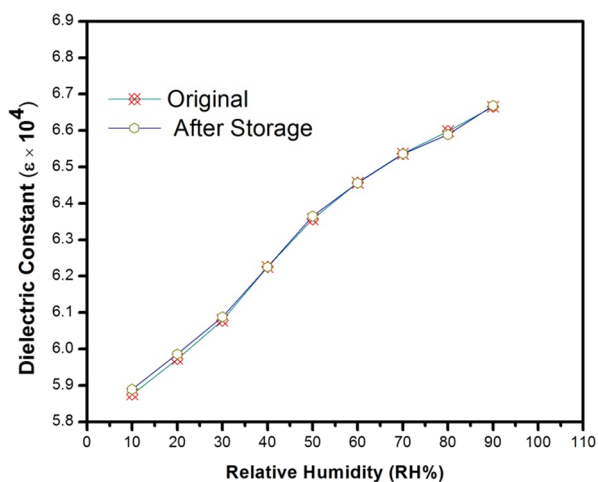


Figure 7. Stability of pure cobalt ferrite nanoparticles calcined at 800 °C. For all data points, the error bars lie within the symbols.

In view of the fact that the large surface-to-volume ratio facilitates the adsorption and desorption process of the water molecules, then the samples of nanosize are high-quality choice to the application of humidity sensors.^{16,19}

DC resistivity response with respect to percentage of %RH of Li-substituted cobalt ferrite nanoparticles measured within the range from 10% to 90% RH at room temperature is shown in Figure 8. It is clear that DC resistivity increases with increasing

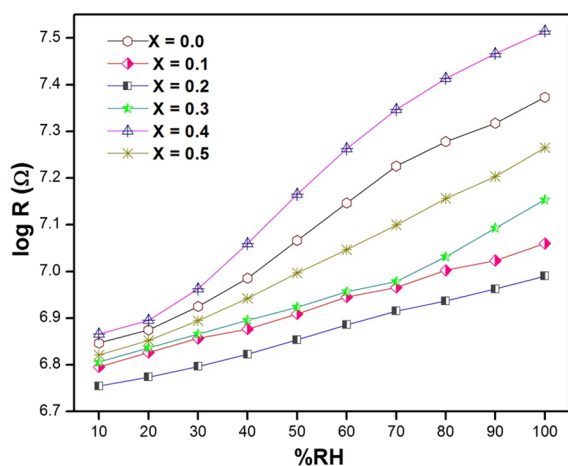


Figure 8. Log R vs %RH of Li-substituted cobalt ferrite nanoparticles at room temperature (x represents the Li concentration).

Li concentration in cobalt ferrite nanoparticles. Thus, the humidity sensitivity of Li-substituted cobalt ferrites increases with increasing relative humidity (%RH). At low relative humidity, the humidity sensitivity of Li-substituted cobalt ferrite samples increases gradually; it is because of the alkali ions that effortlessly contributed the conduction of electrons in ferrites and provided the change in local charge density on the bulk surface to water vapors.²⁰ Accordingly, Li ions uptake oxygen ions from the cobalt ferrite nanoparticles by leaving Co^{2+} ions in bulk form, and it shows that an augmented number of well-pre-arranged adsorption sites furnish elevated surface charge.²¹ For that reason, Li ions give the sites of valences on the surface of ferrite samples and subsequently, humidity sensitivity is high at low relative humidity. From Figure 8, it is observed that DC resistivity decreases up to an $x = 0.2$ concentration of Li, and

then DC resistivity increases with increasing relative humidity; the utmost DC resistivity is observed for the composition $\text{Li}_{0.5}\text{Co}_{0.5}\text{Fe}_2\text{O}_4$. Figure 9 reveals that the connectivity among the

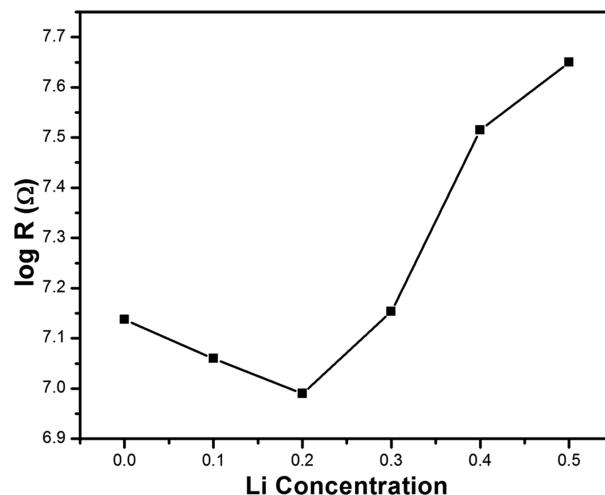


Figure 9. Log R vs Li concentration in cobalt ferrite nanoparticles.

intergrains of metal ions is extremely good and surface area is additionally high; it is because of the less small grains of ferrites with high porosity, leading to the chemisorption and physisorption of water vapors.²²

Figure 10 shows the difference of the humidity sensitivity factor with the Li concentration in cobalt ferrite nanoparticles.

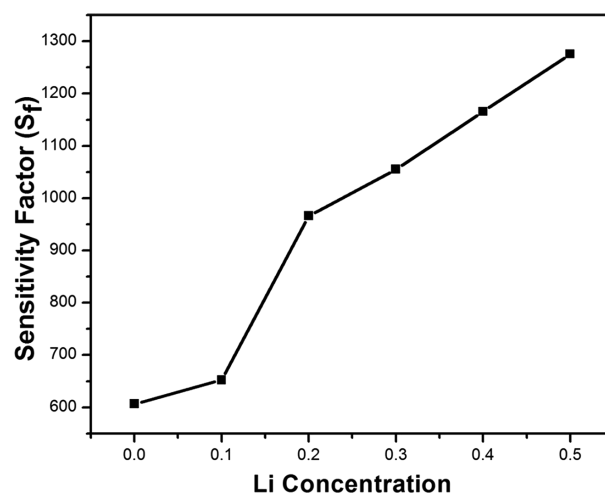


Figure 10. Sensitivity factor vs Li concentration in cobalt ferrite nanoparticles.

However, the sensitivity factor of Li-substituted cobalt ferrite nanoparticles was determined and is listed in Table 1; it is observed that the sensitivity factor increases gradually with increasing Li concentration in cobalt ferrite nanoparticles.²³ As a result, the utmost sensitivity factor $S_f = 1275.64$ was obtained for $\text{Li}_{0.5}\text{Co}_{0.5}\text{Fe}_2\text{O}_4$ nanoparticles. Hence, the sensitivity factor of ferrite nanoparticles is high for the $\text{Li}_{0.5}\text{Co}_{0.5}\text{Fe}_2\text{O}_4$ composition; it is because of the smaller grains, less porosity, and lower surface charge, i.e., advantageous for the top humidity-sensing property of the ferrite nanoparticles.^{10,19,24}

CONCLUSIONS

The result of Li substitution in cobalt ferrite nanoparticles synthesized by a solution combustion method was studied for humidity-sensing properties. From the results, it is observed that nanoscale cobalt ferrite grains formed by the solution combustion method. We reported a large response of the dielectric constant to relative humidity in pure cobalt ferrite and Li-substituted cobalt ferrites. It is observed that Li substitution enhanced the property of humidity sensitivity of the ferrite nanoparticles. The dielectric constants at 90% RH are 6.32 ($x = 0.0$), 6.53 ($x = 0.1$), 6.65 ($x = 0.2$), 6.71 ($x = 0.3$), 6.78 ($x = 0.4$), and 6.90 ($x = 0.5$) for all the concentrations of Li ions in cobalt ferrites. It reveals that as the Li ion concentration increased, the humidity sensitivity of the ferrite nanoparticles also increased. Humidity sensitivity of pure cobalt ferrite was increased with increasing Li concentration. The utmost sensitivity factor $S_f = 1275.64$ was achieved for $\text{Li}_{0.5}\text{Co}_{0.5}\text{Fe}_2\text{O}_4$ nanoparticles, i.e., advantageous for the top humidity-sensing property of the ferrite nanoparticles. These are promising materials for future fabricating new humidity sensors.

EXPERIMENTAL SECTION

AR-grade materials of high purity metal nitrates $\text{Co}(\text{NO}_3)_2$, LiNO_3 , and $\text{Fe}(\text{NO}_3)_3$ are taken in a stoichiometric ratio and dissolved in 50 mL of deionized water. Then, 10% of PVA solution was prepared and also the solution of 30 mg of sucrose dissolved in 50 mL of deionized water and stirred continuously on a magnetic stirrer to get the clear solution of sucrose.¹⁰ Then 10% of PVA solution, metal nitrate solution, and sucrose solution were mixed together and heated on a magnetic stirrer with continuous stirring at an appropriate temperature until NO_2 fumes vanished completely and a gelatinous mixture was formed. This mixture was then heated on a gas burner until it burns like live charcoal for the configuration of ferrite nanoparticles in powder form. The fine powder was calcined at 600 °C for 8 h into the muffle furnace, and then the furnace cooled to room temperature. The calcined powder was added with 2% of PVA, which acts as a binding agent, and then the powder was hard pressed into the shape of pellets using the hydraulic press of 6 tons/inch². The pellets were finally calcined at 800 °C for 10 h and furnace cooled to room temperature.¹⁰

AUTHOR INFORMATION

Corresponding Author

Pradeep Chavan – SB Arts & KCP Science College, Vijayapura, Karnataka 586103, India; orcid.org/0000-0002-1964-4020; Email: cpajju@gmail.com

Complete contact information is available at:

<https://pubs.acs.org/10.1021/acsoomega.0c04784>

Notes

The author declares no competing financial interest.

ACKNOWLEDGMENTS

Author is thankful to MIT Innovation Centre, Manipal for their help and support during the measurement of XRD. Also, the author extends his gratitude to the staff of University Science Instrumentation Center (USIC), Karnatak University Dharwad for the support during the measurement of AFM. This work was not supported by any financial body.

REFERENCES

- (1) Singh, A.; Singh, A.; Singh, S.; Tandon, P. Fabrication of copper ferrite porous hierarchical nanostructures for an efficient liquefied petroleum gas sensor. *Sens. Actuators, B* **2017**, *244*, 806.
- (2) Chen, N. S.; Yang, X. J.; Liu, E. S.; Huang, J. L. Reducing gas sensing properties of ferrite compounds MFe_2O_4 ($\text{M}=\text{Cu}$, Zn , Cd and Mg). *Sens. Actuators, B* **2000**, *66*, 178.
- (3) Zhu, H.; Gu, X.; Zuo, D.; Wang, Z.; Wang, N.; Yao, K. Microemulsion based synthesis of porous zinc ferrite nanorods and its application in a room-temperature ethanol sensor. *Nanotechnology* **2008**, *19*, 405503.
- (4) Li, Z.; Lai, X.; Wang, H.; Mao, D.; Xing, C.; Wang, D. General synthesis of homogeneous hollow core-shell ferrite microspheres. *J. Phys. Chem. C* **2009**, *113*, 2792.
- (5) Singh, S.; Singh, A.; Yadav, B. C.; Tandon, P. Synthesis, characterization, magnetic measurements and liquefied petroleum gas sensing properties of nanostructured cobalt ferrite and ferric oxide. *Mater. Sci. Semicond. Process.* **2014**, *23*, 122.
- (6) Li, X.; Wang, C.; Guo, H.; Sun, P.; Liu, F.; Liang, X.; Lu, G. Double-shell architectures of ZnFe_2O_4 nanosheets on ZnO hollow spheres for high-performance gas sensors. *ACS Appl. Mater. Interfaces* **2015**, *7*, 17811.
- (7) Singh, A.; Singh, A.; Singh, S.; Tandon, P.; Yadav, B. C. Preparation and characterization of nanocrystalline nickel ferrite thin films for development of a gas sensor at room temperature. *J. Mater. Sci.: Mater. Electron.* **2016**, *27*, 8047–8054.
- (8) Benko, F. A.; Koffyberg, F. P. The effect of defects on some photoelectrochemical properties of semiconducting MgFe_2O_4 . *Mater. Res. Bull.* **1986**, *21*, 1183.
- (9) Kulwicki, B. M. Humidity sensors. *J. Am. Chem. Soc.* **1991**, *74*, 697.
- (10) Chavan, P.; Naik, L. R. Effect of Bi^{3+} ions on the humidity sensitive properties of copper ferrite nanoparticles. *Sens. Actuators, B* **2018**, *272*, 28.
- (11) Liu, Y. L.; Liu, Z. M.; Yang, Y.; Yang, H. F.; Shen, G. L.; Yu, R. Q. Simple synthesis of MgFe_2O_4 nanoparticles as gas sensing materials. *Sens. Actuators, B* **2005**, *107*, 600.
- (12) Chavan, P.; Naik, L. R.; Belavi, P. B.; Chavan, G.; Ramesha, C. K.; Kotnala, R. K. Studies on Electrical and Magnetic Properties of Mg-Substituted Nickel Ferrites. *J. Electron. Mater.* **2017**, *46*, 188.
- (13) Li, M.; Cai, G.; Zhang, D. F.; Wang, W. Y.; Wang, W. J.; Chen, X. L. Enhanced dielectric responses in Mg-doped $\text{CaCu}_3\text{Ti}_4\text{O}_{12}$. *J. Appl. Phys.* **2008**, *104*, No. 074107.
- (14) Holc, J.; Slunčko, J.; Hrovat, M. Temperature characteristics of electrical properties of (Ba,Sr)TiO₃ thick film humidity sensors. *Sens. Actuators, B* **1995**, *26*, 99.
- (15) Tao, B.; Zhang, J.; Miao, F.; Li, H.; Wan, L.; Wang, Y. Capacitive humidity sensors based on Ni/SiNWs nanocomposites. *Sens. Actuators, B* **2009**, *136*, 144.
- (16) Arai, H. Semiconductive humidity sensor of perovskite type oxides. *Hyomen Kagaku* **1984**, *5*, 165.
- (17) Li, M.; Chen, X. L.; Zhang, D. F.; Wang, W. Y.; Wang, W. J. Humidity sensitive properties of pure and Mg-doped $\text{CaCu}_3\text{Ti}_4\text{O}_{12}$. *Sens. Actuators, B* **2010**, *147*, 447.
- (18) Kordi Ardakani, H.; Shushtarian, S. S.; Kanetkar, S. M.; Karekar, R. N.; Ogale, S. B. Humidity sensitivity of La^{3+} -doped BaTiO_3 semiconductor thin film deposited by pulsed excimer laser ablation. *J. Mater. Sci. Lett.* **1993**, *12*, 63.
- (19) Shah, J.; Kotnala, R. K. Humidity sensing exclusively by physisorption of water vapors on magnesium Ferrite. *Sens. Actuators, B* **2012**, *171-172*, 832.
- (20) Kotnala, R. K.; Shah, J.; Singh, B.; Kishan, H.; Singh, S.; Dhawan, S. K.; Sengupta, A. Humidity response of Li-substituted magnesium ferrite. *Sens. Actuators, B* **2008**, *129*, 909.
- (21) Reddy, B. M.; Khan, A. Nanosized CeO_2 - SiO_2 , CeO_2 - TiO_2 , and CeO_2 - ZrO_2 mixed oxides: influence of supporting oxide on thermal stability and oxygen storage properties of ceria. *Catal. Surv. Asia* **2005**, *9*, 155.
- (22) Harpster, T. J.; Stark, B.; Najafi, K. A passive wireless integrated humidity sensor. *Sens. Actuators, A* **2002**, *95*, 100.

- (23) Sutka, A.; Pärna, R.; Mezinskis, G.; Kisand, V. Effects of Co ion addition and annealing conditions on nickel ferrite gas response. *Sens. Actuators, B* **2014**, *192*, 173.
- (24) Chavan, P.; Naik, L. R.; Belavi, P. B.; Chavan, G. N.; Kotnala, R. K. *J. Alloys Compd.* **2017**, *694*, 607.